American Mineralogist, Volume 89, pages 382–389, 2004

Identification of pyrite valence band contributions using synchrotron-excited X-ray photoelectron spectroscopy

H.W. NESBITT,[1,*] A.G. BERLICH,[2] S.L. HARMER,[1] I. UHLIG,[2] G.M. BANCROFT,[3] AND R. SZARGAN[2]

[1]Department of Earth Sciences, University of Western Ontario, London, Ontario, N6A 5B7, Canada
[2]Wilhelm-Ostwald-Institut, Fakultät für Chemie und Mineralogie, Universität Leipzig, Linnéstrasse 2, D-O4103, Germany
[3]Department of Chemistry, University of Western Ontario, London, Ontario, N6A 5B7, Canada

ABSTRACT

The major contributions to the pyrite valence band have been identified experimentally by monitoring XPS valence band signal intensity as a function of photon (X-ray source) energy. The S-S σ and σ* orbitals are located at about 13 and 16 eV binding energy and are almost exclusively derived from S 3*s*-S 3*s* mixing; there is no experimental evidence for a S 3*p* contribution to these molecular orbital (molecular orbital) values as required for sp^3 hybridization. Fe-S σ (Fe $3d_{eg}$-S $3p_z$ derived) and Fe-S π and π* (Fe $3d_{t2g}$-S $3p_{x,y}$ derived) molecular orbitals are identified at Binding Energies (B.E.) less than 8 eV, and are consistent with energies calculated by Eyert et al. (1998). Fe-S π molecular orbital contributions are located in the valence band between about 1.8 and 3 eV and Fe-S π* molecular orbitals contribute between about 0.7 to 1.5 eV binding energy. Contributions observed at the top of the valence band and concentrated between the Fermi level and about 0.6 eV B.E. may be derived from Fe $3d_{eg}$ (non-bonding) orbitals. The experimental data are consistent with these non-bonding contributions being derived from surface Fe species (Fe electronic surface states), and perhaps represent the Fe $3d_{eg}$ "dangling bonds" produced by rupture of Fe-S σ bonds during fracture. The conformity of spectral assignments based on experimental data with band theoretical calculations (of Eyert et al. 1998, using a basis set appropriate to pyrite) indicates that the essential aspects of the pyrite valence band are understood and energetically quantified. Additional study is required to identify positively

INTRODUCTION

Burns and Vaughan (1970) proposed that Fe-S molecular orbital (molecular orbital) values occurred in the outer valence band of pyrite which, along with Fe-S σ bonding molecular orbitals, were responsible for the short Fe-S bond length of pyrite. Numerous early theoretical considerations (Goodenough 1972; Li et al. 1974; Bullett 1982; Lauer et al. 1984; Raybaud et al. 1997) indicated that the upper valence band (0 to 2 eV binding energy) was composed of non-bonding (atomic-like) Fe $3d_{t2g}$ orbitals, even though the calculations predicted small S 3*d* and S 3*p* contributions to the upper valence band (their state of mixing was not addressed). Recently, detailed calculations of Eyert et al. (1998), using an appropriate basis set for pyrite, indicated significant π molecular orbital character at the top of the pyrite valence band. In addition to the theoretical considerations, Nesbitt et al. (2002) demonstrated that the Fe^6L^{-1} final state contributed to the top of the valence band thus confirming a significant ligand contribution (and Fe-S orbital mixing) located at the top of the pyrite valence band. The nature of the contribution at the top of the pyrite valence band consequently is uncertain and is the focus of this communication.

Additional ambiguities relate to the nature and location of Fe 3*d*-S 3*p* π bonding contributions in the valence band, the ambiguity arising because these contributions generally have not been discussed or identified in earlier theoretical or experimental studies. The ambiguities are addressed experimentally by collection of pyrite valence band spectra at various photon energies, using synchrotron radiation X-ray photoelectron spectroscopy (SRXPS). The source energy is appropriately tuned to accentuate signals derived from S 3*s*, S 3*p*, Fe 3*d* orbitals, and to accentuate signals derived from localized and delocalized orbitals. An interpretation of bonding and valence band structure is provided which is in accord with results of X-ray emission experiments recently conducted to derive the atom-decomposed partial density of states of pyrite and other sulfides containing inequivalent sulfur sites (Kurmaev et al. 1998).

EXPERIMENTAL ASPECTS

Samples

Pyrite from Soria Spain was used for the experiment and is the same material studied by Mycroft et al. (1990) and Nesbitt et al. (1998; 2000). Laths of pyrite, each with the same orientation, were cut from a large sample with the long axis of each lath parallel to the **c** axis of the mineral. Each lath was fractured sub-parallel to the (001) plane in the introduction chamber of the synchrotron-based and conventional XPS instruments used in the study.

The binding energies of crystal orbitals vary somewhat depending on their orientation relative to the crystallographic axes of the crystal, as shown in Figure 1 (discussed subsequently). There is consequently a need to know the orientation of the crystal if highly accurate deconvolution of orbital energies is to be achieved (Hüfner 1995). Such studies are almost impossible for minerals such as pyrite which do not cleave readily. Fracture of pyrite leaves a rough or conchoidal surface with exposed faces having different orientations. XPS valence bands collected from these surfaces provide an "averaged" DOS signal with weighting favoring (001) surfaces. The lack of perfect cleavage precludes detailed probing of the Density of States (DOS) and its relationship to Brillouin zones. Four different surfaces were prepared for these studies, and although each surface was fractured sub-parallel to the (001) face, minor differences may arise due to the signal being weighted slightly differently.

* E-mail: hwn@uwo.ca

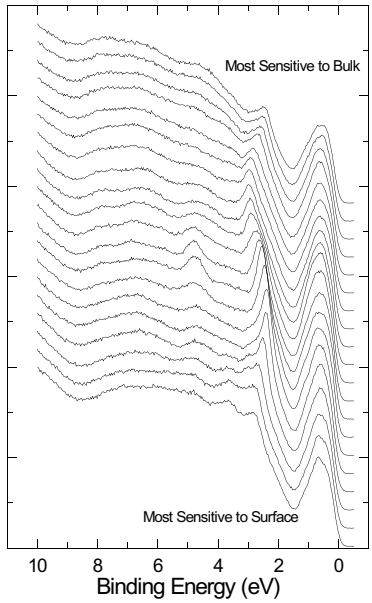

FIGURE 1. Angle-resolved X-ray photoelectron spectra of a conchoidally fractured pyrite surface approximately normal to (001). Take-off angle is minimum for the top spectrum and is maximum for the spectrum plotted at the bottom of the stack.

INSTRUMENTAL AND ANALYTICAL ASPECTS

The pyrite structure was determined by powder X-ray diffraction study using a Rigaku instrument with a Cu*K*α source. Electron microprobe analyses were conducted with a JOEL JXA-8600 Superprobe (U.W.O), revealing a composition close to ideal (FeS_2). No impurities were detected at a 0.1 wt% level.

One pyrite lath was fractured in the analytical chamber of a Kratos Ultra Axis XPS instrument (base pressure of 10^{-8} Pa) with a monochromatized Al*K*α source. The exposed surface was immediately analyzed (1487 eV source energy) with the results shown in Figure 2a. The spectrum was collected at about 1×10^{-8} Pa, a 10 eV pass energy and with a standard "Kratos" slit (equivalent to a 300 µm spot size).

The 100, 80, and 30 eV spectra (Figs. 2b, 2c, and 2e) were collected from one lath, fractured under the vacuum (about 10^{-7} Pa) of the introduction chamber attached to a SCIENTA SES 200 analyzer (Synchrotron Radiation Center, Wisconsin). After fracture, samples for SRXPS analysis were transferred to the SCIENTA analyzer chamber (base pressures of 10^{-8} Pa) and spectra were collected immediately after the beam was focused. Monochromater resolution (*E*/*dE*) was either 17000 or 10000 with a pass energy of 10 eV, giving an electron resolution better than 20 meV. The three spectra (100, 80, and 30 eV spectra) were collected sequentially using the PGM line at SRC. The spectra were collected from the same surface with the same orientation, so that changes to signal intensity are solely a response to changes in source energy. Spectra were taken at ambient temperature and at a take-off angle of 78°.

The 50 eV spectrum (Fig. 2d) was collected from a third pyrite lath (fractured normal to the **c** axis) using the PGM beam line and SCIENTA SES 200 analyzer at the Synchrotron Radiation Center (see Nesbitt et al. 2002 for details). The valence band spectrum collected at He(I) photon energy (21.2 eV), and here illustrated in Figure 2f, was taken from the study of Pettenkofer et al. (1991). The spectrum was again collected from a (001) surface. Experimental conditions pertaining to its collection may be found in the reference. The top of the valence band of each spectrum was aligned with that of Figure 2a and the spectrum of Figure 2a was standardized to the Au 4*f* line (84.00 eV) and calibrated using the Cu $2p_{3/2}$ and Cu 3*s* orbital energies of Cu metal.

STRUCTURE AND VALENCE BAND PROPERTIES

Structure

Pyrite displays rocksalt structure where Fe replaces Na and S dimers replace Cl. The mid-point of the S-S internuclear axis coincides with the Cl lattice position. Each sulfur dimer has its internuclear axis oriented parallel to the unit cell body diagonals with dimer axes of alternating sulfur layers aligned parallel to different diagonals.

Fe is octahedrally coordinated with the octahedron compressed somewhat along a trigonal axis (S_6 symmetry) and these complications yield a *Pa*3 space group. Each S atom of the S-S dimer is tetrahedrally coordinated to three Fe atoms and an adjacent S atom. The "tetrahedron" is appreciably distorted due in part to the shorter S-S bond length (2.08 Å) and longer Fe-S bond lengths (2.26 Å).

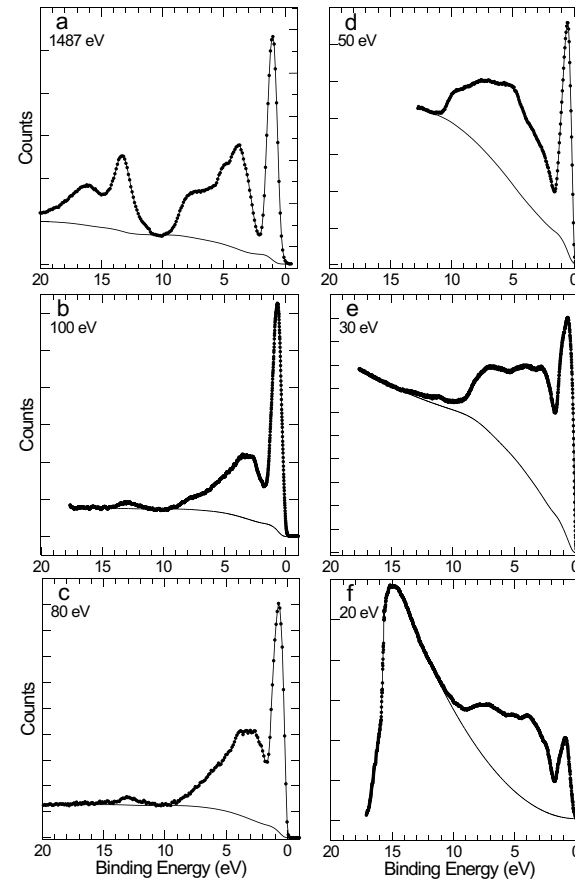

FIGURE 2. XPS spectra of the pyrite valence band collected at the photon energy indicated in each diagram. The ordinate is (count rate) and is scaled arbitrarily. The data of Figure 2**a** were collected at Surface Science Western using an Al*K*α source. The spectrum of Figure 2**f** is reproduced from Pettenkofer et al. (1991) who collected it with a He(I) lamp (21.1 eV photon energy). All other spectra were collected at the Synchrotron Radiation Center (Stoughton, Wisconsin).

Photoionization cross sections

The likelihood of excitation of a photoelectron from an orbital is dependent upon the orbital angular momentum, orientation, and dispersion (localization) of the orbital in a solid (Yeh and Lindau 1985). As a result, the peak intensity derived from a specific orbital may be varied by appropriate choice of photon energy (Fig. 3). At about 20 eV, Fe 3*d* and S 3*p* photon-capture cross-sections are similar but at about 35 eV photon energy the

Fe 3*d* cross-section is more than tenfold greater than the S 3*p* cross-section (Fig. 3b). At greater photon energies, the S 3*p* cross-section again approaches the Fe 3*d* cross-section so that at 1487 eV photon energy the ratio, Fe 3*d*/S 3*p*, is about 2:1. The S 3*s* orbital cross-section is much smaller than either the Fe 3*d* or S 3*p* at 20 eV photon energy, but the S 3*s* cross section approaches those of the other two at 1487 eV.

The intensities of photopeaks derived from S 3*p* and Fe 3*d* valence orbitals cannot be predicted quantitatively from photoionization cross-sections for numerous reasons. The cross sectional dependence on photon energy is based on atomic orbital photoionization cross sections (Yeh and Lindau 1985) and molecular orbitals derived from Fe 3*d*-S3*p* mixing may have somewhat different cross-sections depending on the extent of molecular orbital delocalization. In spite of this, dependence of atomic orbital cross sections on photon energies provides a reasonable guide to intensities of valence band contributions, especially above about 50 eV photon energy (Gelius 1974; Bancroft and Hu 1999). Although not quantitative, these data are the first substantive experimental test of pyrite valence band theoretical calculations. In the future, and with additional detailed study, molecular orbital cross-sections of the pyrite valence band data can be made quantitative.

Surface and bulk contributions

The sensitivity of XPS spectra to surface layers is dependent in part upon photon energy (Briggs and Seah 1990; Tanuma et al. 1991). Maximum surface sensitivity is obtained where the photon energy is between about 40 and 100 eV and for such energies photoelectrons are derived primarily from the top two atomic layers of a solid. At lower and higher photon energies, photoelectrons are derived from deeper layers so that at 1487 eV photon energy, about 10 atomic layers are sampled. The valence band results presented here include both highly surface sensitive and bulk sensitive spectra and their interpretation necessarily includes consideration of the surface and bulk sensitivity of the spectra.

Backgrounds

Background intensities vary greatly depending on the photon energy and detailed comparison of spectra collected at different energies requires subtraction of background from spectra. The spectra and the background calculated for each is illustrated in Figure 2. Background simulation is achieved by combining a Shirley and quadratic contribution (Shirley 1972). The valence band spectra, with background removed, are plotted in Figure 4 and the resulting spectra are the basis for subsequent interpretation.

Terminology, peak intensities, and photon energies

The pyrite valence band is conveniently subdivided into an outer and an inner valence band separated by a minimum near 2 eV (Fig. 4). The inner valence band extends from the minimum to about 20 eV binding energy. The outer valence band is characterized by a strong lone peak centered between about 0.6 and 1 eV. Binding energies of electrons contributing to the valence band of a single crystal are "k" dependent and may yield photoelectrons of different kinetic energy depending on the polar and azimuthal angle of emission relative to the crystallographic axes of the mineral (Brillouin Zones). Photoelectrons from a specific molecular orbital consequently may display a rather broad range of binding energies depending on the exciting photon energy or electron emission angle. Nevertheless, distinct "peaks" may be identified.

Angle-Resolved Ultra-Violet Spectra of a conchoidal surface approximately normal to (001) were collected using He(I) radiation (21.2 eV) on a VG ESCALAB 250 instrument to investigate directional properties of the valence band peaks. The sample was fractured in the vacuum of the introduction chamber, immediately transferred to the analytical chamber and the shallowest angles collected first; see Mycroft et al. (1995) for details of the technique. The results (Fig. 1) illustrate that the highest binding energy "peak" of the inner valence band varies somewhat as a function of take-off angle. Although a second peak within the interior of the inner valence band is sharpened appreciably at two angles, most peaks are little affected by take-off angle, perhaps because the conchoidal fracture exposes a sufficient number of orientations to yield an "averaged" signal.

Seven contributions (peaks) can be identified in most of the spectra of Figure 4 (peaks labeled a through g). They are located near 0.8 eV (peak "a"), 2.5 eV (peak "b"), 4 eV (peak "c"), 5 eV (peak "d"), 7 eV (peak "e"), 13 eV (peak "f"), and 16 eV (peak "g"). The nature of the orbital contributions giving rise to the peaks may be evaluated (qualitatively) by relating peak intensities at specified photon energy to the S 3*p* and Fe 3*d* photoionization cross sections (Fig. 3) as now discussed.

From the cross sections, peaks of greatest S 3*p* character

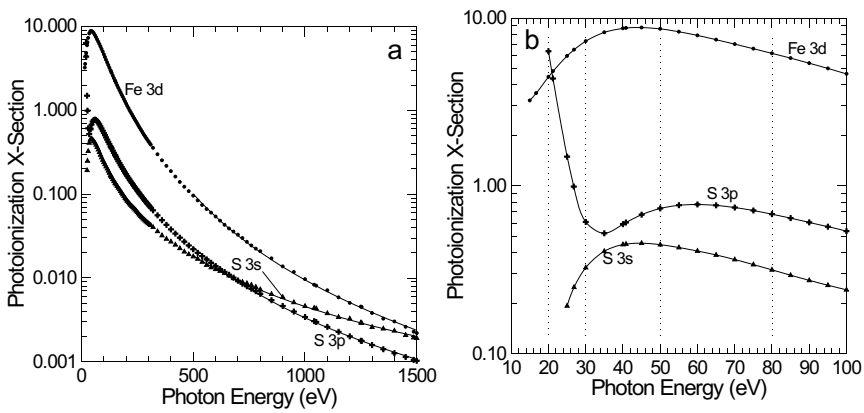

FIGURE 3. (**a**) S 3*s*, S 3*p*, and Fe 3*d* atomic subshell photoionization cross sections as a function of photon energy (source energy) in the region 0 to 1500 eV (data from Yeh and Lindau 1985). (**b**) Cross sections for the same subshells in the energy range 10 to 100 eV photon energy. Dashed lines indicate photon energies at which spectra were collected.

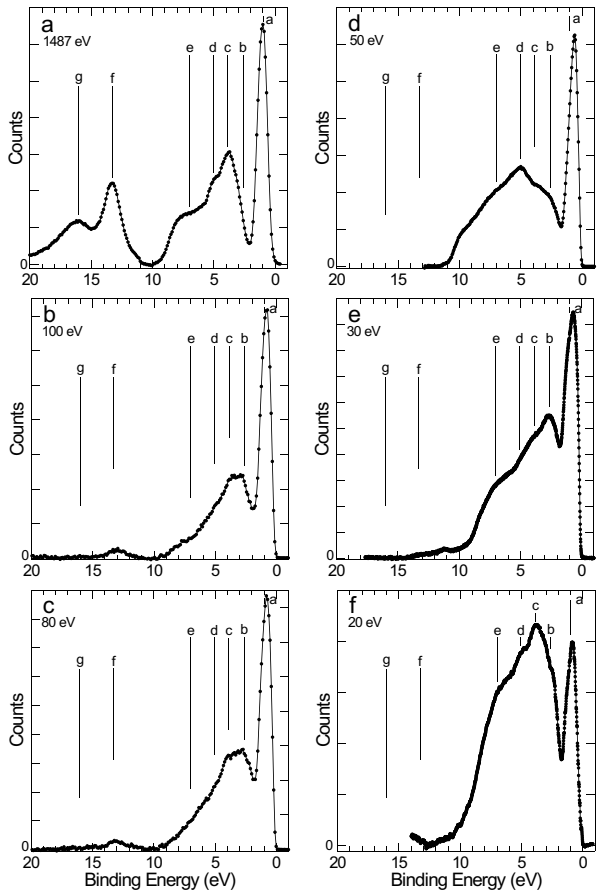

FIGURE 4. XPS spectra of Figure 2 with backgrounds removed. Backgrounds were simulated partly as Shirley and partly as quadratic in nature (see text for details). The vertical lines indicate "peaks" observed in numerous spectra. These "peaks" are more accurately referred to as bands that are concentrated within a narrow binding energy range.

should be most enhanced in the 20 eV spectrum (Fig. 4f) whereas peaks with strong Fe 3*d* character should be most enhanced in the 30 eV spectrum (Fig. 4e) and S 3*s*-derived peaks most prominent in the 1487 eV spectrum (Fig. 4a). From comparison of the spectra of Figure 4, it can be concluded that peak "c" (strongly enhanced in Fig. 4f) and peak "b" (strongly enhanced in Fig. 4e) are respectively of strong S 3*p* and Fe 3*d* character. The "b/c" ratio decreases in spectra collected at progressively greater photon energy (30, 80, 100, and 1487 eV) in accordance with the decreasing Fe3*d*/S3*p* cross section ratio. The 50 eV spectrum is least reliable as an indicator of the orbital character of the peaks because of resonance effects related to promotion of Fe 3*p* electrons into empty Fe 3*d* orbitals (Nesbitt et al. 2003; Lad and Henrich 1989). Although the Fe 3*p*-3*d* resonance energy is 53.5 eV, there are both pre- and post-resonance effects that may affect the signal.

SPECTRAL INTERPRETATION AND PEAK ASSIGNMENTS

Peaks "f" and "g"

The 1487 eV valence band spectrum of pyrite displays a doublet between 20 and 10 eV (Fig. 4a, peaks "f" and "g"). Van der Heide et al. (1980) attributed these peaks to S-S σ (S3*s*-S3*s*) and σ*(S3*s*-S3*s*) molecular orbitals which are respectively bonding and antibonding. The assignment is confirmed by the relationship between cross sections and peak intensities. The S 3*s* cross-section is similar to the Fe 3*d* and S 3*p* cross-sections at 1487 eV source energy (Fig. 3) and peaks "f" and "g" are strong just as is peak "a" (a peak with strong Fe 3*d* character as discussed subsequently). The "f" and "g" signals are, however, very weak or absent in the 100, 80, and 30 eV spectra (Figs. 4b, 4c, 4e) whereas the intensity of peak "a" remains strong. At 100, 80, and 30 eV photon energies, the S 3*s* cross section is tenfold less than the Fe 3*d* cross section; the observed weakness of peaks "f" and "g" relative to peak "a" is therefore explained by changes in S 3*s* and Fe 3*d* cross-sections as a function of photon energy. The expected correlation between ionization cross section and peak intensity confirms that the 16 and 13 eV peaks are S 3*s*-derived molecular orbitals, as deduced by van der Heide et al. (1980).

Van der Heide et al. (1980) proposed S 3*s* and S 3p_z orbital mixing leading to sp^3 hybridization on S atoms and to their approximately tetrahedral coordination in pyrite. The proposed 75% S 3*p* contribution to the σ and σ* signals at 13 and 16 eV binding energy should yield a detectable signal in most spectra of Figure 4. Although other peaks with S 3*p* character are apparent in the 30 eV spectrum (discussed subsequently), there is no contribution at 13 or 16 eV binding energy. As additional evidence, the σ* signal is very weak in the 100 and 80 eV spectra (Fig. 4b, peak f) and the σ signal is not detected; it should be if S 3*p* hybridization occurs equally in the σ and σ* molecular orbitals. These observations make questionable the assumption of 75% S 3*p* contribution to the homopolar S-S σ molecular orbitals, and the common use of sulfur sp^3 hybridization to explain the approximately tetrahedral coordination of sulfur is not supported by these XPS spectra. Instead the XPS data indicate that peaks "f" and "g" (σ and σ* bonds) are almost entirely of S 3*s* character. The conclusion is well supported by aligning the SKβ X-ray emission spectra of pyrite to the binding energy scale: there is no indication for $3p \rightarrow 1s$ transitions in the energy region above 10 eV BE (Kurmaev et al. 1998).

Apparently, the hybridization concept cannot be used to explain the tetrahedral geometry associated with sulfur bonding in pyrite.

Peak "e" (7 eV)

The 7 eV contribution appears in the 1487 and 20 eV spectra as a strong, broad shoulder on the 5 eV peak (Figs. 4a, 4f). The 7 eV peak is, however, exceptionally weak or absent in Figures 4b and 4c, spectra in which Fe 3*d* signals are accentuated. The experimental results therefore indicate a strong S 3*p* orbital contribution to peak "e" with negligible Fe 3*d* contribution.

Eyert et al. (1998) calculated (for the first time) both the Density of States (DOS) *and* the Crystal Orbital Overlap Populations (COOP) for pyrite. (The COOP is effectively the bonding and antibonding molecular orbital contributions to the valence band.) Their results (pertinent to this communication) are reproduced in Figure 5. Two major COOP bonding peaks occur between 6 and 7 eV binding energies (Fig. 5c) and were interpreted by Eyert et al. to be σ bonds derived from mixing of S 3p_z orbitals

(to produce the S-S dimer of the mineral). The theoretical considerations and XPS data are therefore in accord, both indicating that the 7 eV peak results from mixing of S 3*p* atomic orbitals to form σ bonding molecular orbitals. Eyert et al. (1998) calculate the σ* antibonding counterpart to be located in the conduction band between –3 and –4 eV binding energies (Fig. 5c, labeled σ*[S-S]). This is a homopolar bond and the σ and σ* molecular orbitals are separated by about 10 eV, indicating strong orbital overlap. It is the molecular orbital primarily responsible for the sulfur dimeric species in pyrite.

Peak "d" (5 eV)

The 5 eV peak is the second most intense contribution to the inner valence band in the 20 and 1487 eV spectra, signifying a strong S 3*p* contribution. The peak is weaker in the 80 and 100 eV spectra, indicating weak or negligible Fe 3*d* contributions. The 30 eV spectrum (Fig. 4e) displays a shoulder at 5 eV which is appreciably less intense than the 2.5 eV peak (peak "*b*"), again suggesting a weak Fe 3*d* contribution at 5 eV. The most intense peak of the inner valence band of the 50 eV spectrum is at 5 eV. Again, resonance contributions (maximum effects near 53.5 eV) make interpretation of these data ambiguous. The XPS data suggest peak "d" has a strong S 3*p*-derived orbital contribution and weak or negligible Fe 3*d* contribution.

Eyert et al. (1998) indicate a S-S π bond contribution between 5 and 6 eV derived from mixing of S $3p_{x,y}$ atomic orbitals (Fig. 5c). The binding energy and strong S 3*p* character of peak "d" suggests it corresponds with the S-S π bonding contribution calculated by Eyert et al. (1998). They calculate the antibonding counterpart to be located between 2 and 3 eV binding energy (Fig. 5c, antibonding contribution labeled π*[S-S]). Both π and π* orbitals are within the inner valence band, hence fully occupied. These bonds therefore do not contribute to the strength of the S-S dimeric bond and more likely destabilize it somewhat.

Peak "c" (4 eV)

This is the most prominent peak of the 20 eV spectrum and of the inner valence band of the 1487 eV spectrum, indicating a strong S 3*p*-derived orbital contribution. There are, however, Fe 3*d* contributions at this energy, as indicated by shoulders in the 100, 80, 50, and 30 eV spectra; peak "c" apparently represents mixed Fe 3*d*-S 3*p* molecular orbital contributions. Comparison with the intensities of peaks "b" and "c" in the 20 and 30 eV spectra (Figs. 4e, 4f) demonstrates that there is more S 3*p* character in peak "c" than in peak "b".

Eyert et al. (1998) calculate Fe-S σ bonds (Fe $3d_{eg}$-S 3*p*-derived) to be concentrated between 3 and 4 eV binding energy (Fig. 5c). The calculated energy range corresponds to peak "c" of the XPS spectra (Fig. 4). The calculations and XPS data are therefore consistent and we conclude that peak "c" represents σ bonding molecular orbitals. Their bonding nature implies stronger S 3*p* than Fe 3*d* character, a quality consistent with the XPS data. Their σ* (antibonding) counterparts are calculated to be in the "conduction band" (Eyert et al. 1998). These bonds are the major contributors to Fe-S bond strength in pyrite, and are largely responsible for the short Fe-S bond length.

Peak "b" (2.5 eV)

Peak "b" is the strongest peak of the inner valence band in the 30, 80, and 100 eV spectra, all spectra where the Fe 3*d* cross-section is strongly enhanced over those of S 3*p* orbital cross section. We conclude that this peak has strong Fe 3*d* character. The 20 eV spectrum (Fig. 4f) displays, however, an appreciable shoulder at 2.5 eV binding energy, and a weak shoulder is observed in the 1487 eV spectrum (Fig. 4a), indicating that there is some S 3*p* character to this peak; the contributions to this peak likely are molecular orbitals of mixed Fe 3*d*-S 3*p* character. The character of peak "b" differs somewhat from that of peak "c" in that the former is of greater Fe 3*d* character and the latter of greater S

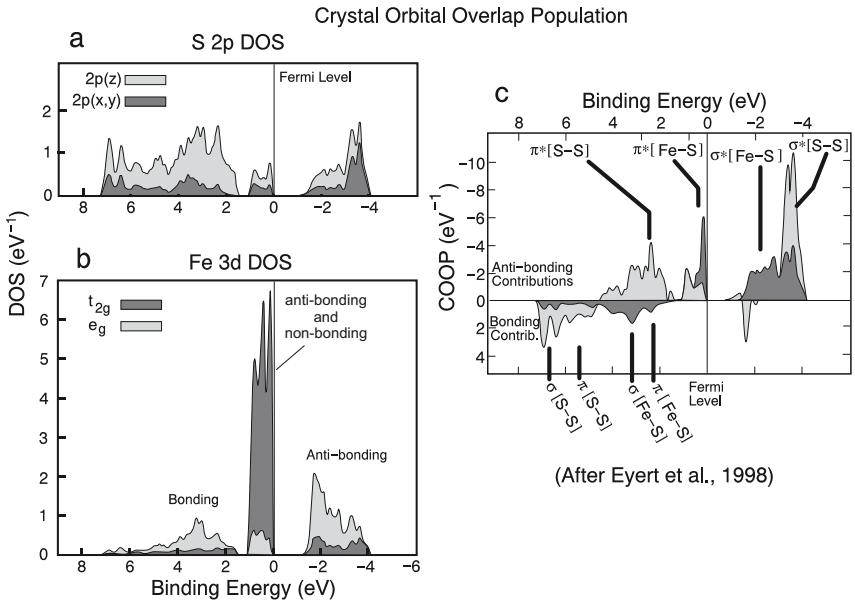

FIGURE 5. S 3*p* and Fe 3*d* orbital contributions to the valence band Density of States (DOS) are illustrated in Figures 5**a** and 5**b**. The Crystal Orbital Overlap Populations (COOP) are direct indication of the nature of the molecular orbital bonding and antibonding contributions to the valence band (Fig. 5**c**). The diagrams are modified after Eyert et al. (1998).

3*p* character, as now emphasized.

Simulations prior to that of Eyert et al. (1998) proposed that the only Fe 3*d*-S 3*p* derived molecular orbitals to contribute to the inner valence band were of σ symmetry (Fe $3d_{eg}$-S 3*p* mixing) as noted, for example, by Raybaud et al. (1997); thus by these calculations, peaks "b" and "c" should arise from mixing of the same molecular orbitals and in similar proportion, an interpretation inconsistent with the XPS data just discussed.

Eyert et al. (1998), using a large basis set for pyrite, were the first to propose Fe-S π and π* molecular orbital contributions (Fe $3d_{t2g}$- and S $3p_{x,y}$-derived), where the S $3p_{x,y}$ atomic orbitals are first mixed to produce S-S π and π* orbitals, and the higher energy π* orbitals are then mixed with Fe $3d_{t2g}$ atomic orbitals to produce Fe-S bonding and antibonding molecular orbitals of π and π* symmetry. Eyert et al. (1998) calculate the Fe-S π bonding contribution to contribute mostly to the top of the inner valence band and the antibonding molecular orbitals to contribute primarily to the outer valence band (Fig. 5c). The XPS data, and the character of peak "b" are consistent with the simulation of Eyert et al. (1998) and we conclude that peak "b" is primarily an Fe-S π bond contribution as proposed by Eyert et al. (1998). The interpretation is also consistent with the nominally more ionic Fe-oxyhydroxides where the Fe 3*d* bands contain appreciable O 2*p* character attributable to the covalence of the Fe-O bond (Sherman 1985; Todd et al. 2003).

The Fe-S π and π* orbitals are filled so they do not contribute to bond number or strength. The short Fe-S bond length in pyrite (2.26 Å) may promote, and explain formation of these Fe-S π-symmetric molecular orbitals. The small difference in energy separating the π and Fe-S π* orbitals (less than 2 eV) implies that metal-ligand orbital overlap is minimal; about 2 eV separates the (parental) Fe $3d_{t2g}$ (non-bonding) and π* orbitals (S-S $3p_{x,y}$-derived).

Peak "a" (outer valence band)

The outer valence band consists of one intense peak (Fig. 4a, peak "a"). Relative to the inner valence band (2 to 20 eV), the outer valence band peak intensity is greatest in the 30, 50, 80, and 100 eV spectra (Figs. 4b,c, and d) and weakest in the 20 eV spectrum (Fig. 4f). From these data, and the Fe 3*d* and S 3*p* cross-sectional dependence on photon energy, we conclude that the outer valence band is largely of Fe 3*d* character. The peak, however, displays complexity which is not readily explained if only Fe 3*d* orbitals contribute to this peak.

The outer valence band of the 80, 30, and 20 eV spectra (Fig. 6) varies in position and shape as a function of photon energy. Peak "a" of the 20 eV spectrum has a maximum at slightly greater than 0.8 eV binding energy, the 80 eV spectral maximum is slightly less than 0.8 eV, and the maximum is shifted to about 0.65 eV in the 30 eV spectrum. The binding energy dependence on photon energy is independently confirmed by the data of Pettenkofer et al. (1991). For their data, the maximum in peak "a" is shifted to lower binding energy in their spectrum collected at 41 eV (HeII source) than in their 20 eV spectrum (Fig. 6, HeI source).

In addition to a shift in peak maximum, the peak changes shape. The spectral intensity on the low binding energy side of peak "a" increases systematically with increase in both surface sensitivity and with increase in the Fe 3*d* cross section (Fig. 6). The 20 eV spectrum is least surface sensitive and also is least sensitive to the Fe 3*d* signal. The 30, 41, and 80 eV spectra are appreciably more surface sensitive and are much more sensitive to the Fe 3*d* signal relative to the S 3*p* signal.

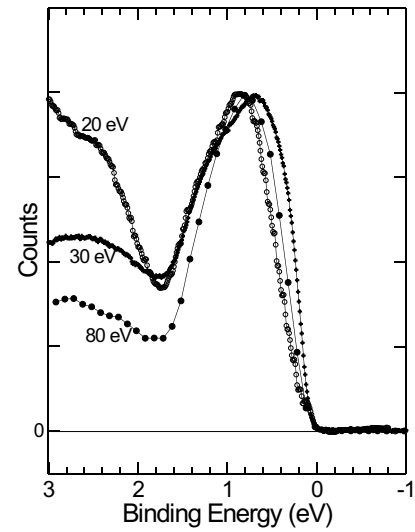

FIGURE 6. Expanded view of the outer valence band spectra collected at 20, 30, and 80 eV photon energy (spectra are background corrected). The peak maximum of the outer valence band shifts to lower binding energy and becomes broader with increases surface sensitivity and with greater sensitivity to the Fe 3*d* signal.

The sympathetic relationship among surface sensitivity, Fe 3*d* signal sensitivity and spectral intensity between 0 and 0.6 eV (Fig. 6) suggests that the signal in this binding energy range is primarily a surface contribution of Fe 3*d* character. By implication the region between 0.7 and 2 eV has a somewhat greater S 3*p* contribution (although not dominant). A previous resonant XPS study confirms that there is S 3*p* character in peak "a" and that a portion of this signal likely is derived from Fe surface states (Nesbitt et al. 2003).

The experimental data suggest that the Fe-S π* molecular orbitals previously discussed (see section on peak "b") contribute primarily to the high binding energy side of peak "a" (centered at about 1 eV) and that Fe 3*d* orbitals of surface Fe atoms contribute more to the low binding energy side of peak "a" (centered at about 0.5 eV). The simulation of Eyert et al. (1998) does not consider surface contributions, thus the Fe 3*d* surface state contribution to peak "a" cannot be substantiated by their calculations. Furthermore, this surface contribution defines the top of the valence band where a surface electronic state is expected. Additional detailed experimental work is thus required to test the hypothesis that the top of the valence band results primarily from Fe 3*d* (non-bonding) surface contributions and this is the subject of a future communication.

Band/molecular orbital model

Derivation. A valence band model for pyrite is summarized qualitatively in Figure 7. The 1487 eV valence band spectrum

(Fig. 4a) is reproduced at the left of Figure 7 and the band model is an attempt to interpret the various features of, and contributions to, the spectrum. The binding energy of the Fe $3d_{t2g}$ atomic orbitals (low spin, octahedral coordination) is illustrated, with the Fe $3d_{eg}$ (d^{z^2}) atomic orbitals separated from it by Δ, the ligand field splitting energy (Bronold et al. 1994; Nesbitt et al. 2000). The sulfur S 3*s* and S 3*p* atomic orbital energies are displayed (qualitatively) and the origins of the σ and π bonding and antibonding molecular orbitals for the S dimer are also shown. The molecular orbitals are broadened into binding energy bands (shaded or patterned rectangular areas) as must occur in solids. The molecular orbital configuration for disulfide (S_2^{2-}) shown in Figure 7 is taken from van der Heide et al. (1980). Their interpretation, however, has the S 3*p*-derived σ bond located energetically lower than the π bonds, whereas Kühne et al. (1984) place the σ bond at higher energy than the π bonds. Kühne et al. (1984) offered no explanation for the difference but these experimental results support the interpretation of van der Heide et al. (1980).

The origin of bonding and antibonding σ and π molecular orbitals derived from mixing of Fe 3*d* and S 3*p* atomic orbitals is also shown on Figure 7. These molecular orbitals are also broadened into bands (patterned and shaded rectangles) to demonstrate that these orbitals span a range of binding energies, as expected in a solid. Of particular importance to this communication are the Fe-S π and π^* [Fe $3d_{t2g}$-S $3p_{x,y}$ (π^*-derived)] molecular orbitals near the top of the valence band, and their origin requires some explanation. Because all S 3*p* orbitals are involved in S_2^{2-} molecular orbitals, only the S-S π^* (S $3p_{x,y}$-derived) orbitals are of correct symmetry and orientation to mix with Fe $3d_{t2g}$ orbitals and their mixing form the Fe-S π and π^* molecular orbitals (bands) near the top of the valence band. Molecular Orbital contributions to the top of the valence band was anticipated by Burns and Vaughan (1970) and, although of different origin, molecular orbital contributions at the top of the valence band have been confirmed here and by experimental investigations via $SL_{2,3}$ X-ray emission spectra (Kurmaev et al. 1998).

Also illustrated in Figure 7 is the Fe $3d_{eg}$ surface state. Its binding energy is somewhat less than that of Fe $3d_{t2g}$ atomic orbitals, as explained by Bronold et al. (1994) and Nesbitt et al. (1998; 2000). These XPS data suggest that Fe $3d_{eg}$ surface state overlaps with, but extends to somewhat greater energy than, the Fe-S π^* antibonding orbitals (Fig. 7). The Fe $3d_{eg}$ surface state consequently is shown to define the top of the valence band. As argued by Bronold et al. (1994) and Nesbitt et al. (1998; 2000), Fe-S σ molecular orbital bond scission will produce Fe $3d_{eg}$ non-bonding orbitals (surface states) at the fracture surface. These will be stabilized relative to the other Fe 3*d* orbitals resulting in an electron occupying the orbital. Additional detailed valence band studies are required to confirm the outer valence band assignments, and particularly to confirm that Fe $3d_{eg}$ surface states define the top of the valence band of pyrite.

Implications. The XPS data indicate that peak "c" has stronger S 3*p* character than peak "b", the latter peak having stronger Fe 3*d* character. The difference in character and implications are consistent with the calculations of Eyert et al. (1998) who find Fe-S σ bonds contributing most near 4 eV whereas the Fe-S π and π^* molecular orbitals contribute most at about 2.5 eV and between 0.7 and 2 eV. Peak "b" contributions cannot be readily interpreted as Fe-S σ or σ^* molecular orbitals, as proposed by most older calculations (Bullett 1982; Lauer et al. 1984; Holzwarth et al. 1985; Folkerts et al. 1987; Temmerman et al. 1993; Raybaud et al. 1997).

Whereas most simulations attribute the outer valence band to Fe $3d_{t2g}$ non-bonding orbitals (Bullett 1982; Lauer et al. 1984; Holzwarth et al. 1985; Folkerts et al. 1987; Temmerman et al. 1993; Raybaud et al. 1997; Rosso et al. 1999), calculations of Eyert et al. (1998) indicate primarily Fe-S π^* molecular orbital contributions to the outer valence band. The XPS data indicate Fe-S π molecular orbital formation, thus supporting the simulation of Eyert et al. The XPS data, however, also suggest Fe 3*d* non-bonding contributions at the top of the valence band. Their presence may result from bond scission during fracture (Fe surface electronic states produced) because scission leaves some Fe atoms under-coordinated at the surface with the ruptured molecular orbitals reverting to non-bonding states. Bond scission leaves the Fe $3d_z2$ non-bonding orbitals as the highest energy orbitals of the pyrite valence band (Bronold et al. 1994; Nesbitt et al. 1998, 2000). These "dangling bonds" are conse-

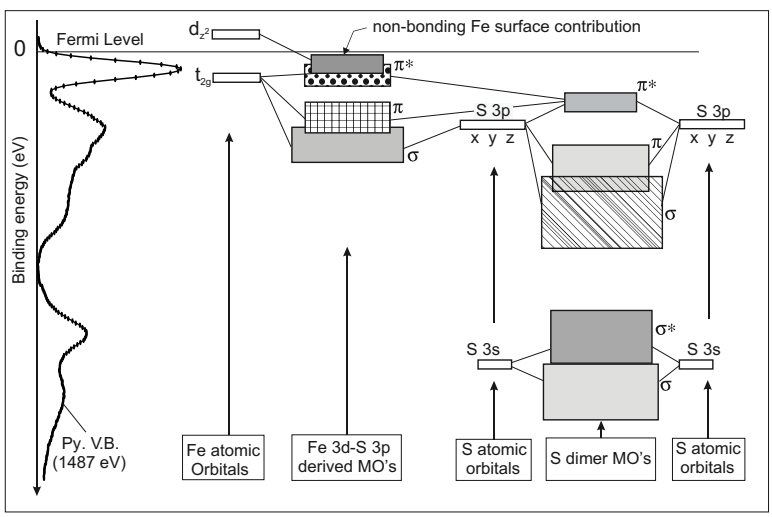

FIGURE 7. A band model of the pyrite valence band illustrating the approximate range of binding energies over which the bands extend, and their atomic and molecular orbital origins. The patterned and shaded rectangles (labeled according to symmetry and bond type) represent the various bands contributing to the spectrum. The band model for the S-dimer contributions is derived from the molecular orbital model of van der Heide et al. (1980). The Fe $3d_{eg}$ and Fe $3d_{t2g}$ atomic orbital splitting and other aspects are taken from Bronold et al. (1994) and Nesbitt et al. (2000). The XPS valence band of pyrite, shown at the left of the diagram, was collected at 1487 eV (Fig. 4a). The indicated non-bonding Fe surface contribution is not a molecular orbital contribution, but is included to complete the band contributions

quently the least stable electronic states contributing to the top of the outer valence band. Furthermore, they are most likely to be detected in spectra collected at 30 to 100 eV where surface state contributions approach 40 to 50% of total signal (Leiro et al. 1998; Schaufuss et al. 2000; Nesbitt et al. 2000; Nesbitt et al. 2002). The hypothesis requires confirmation.

ACKNOWLEDGMENTS

We thank two reviewers, one of whom was D. Sherman, for insightful reviews and suggestions to improve the manuscript. Experiments were conducted at Surface Science Western (SSW), at the Earth Science Department (U.W.O.), and at the Synchrotron Radiation Center (SRC), University of Wisconsin-Madison. The study was supported by National Science and Engineering Research Council of Canada grants to H.W.N. and G.M.B., a BMBF (Germany) grant to R.S., and by NSF under Award No. DMR-00884402. We thank H. Höchst, S. McIntyre, and R. Davidson for technical support while at SRC and SSW, and A. Pratt and W. Skinner for their help during collection of the spectra.

REFERENCES CITED

Bancroft, G.M. and Hu, Y.F. (1999) Photoelectron Spectra of Inorganic and Organometallic molecules in the gas phase using synchrotron radiation. In E.I. Solomon and A.B.P. Lever, Eds., Inorganic Electronic Structure and Spectroscopy, 1, 443–512. Wiley, New York.

Briggs, D. and Seah, M.P. (1990) Practical Surface Science, 657 p. Wiley, Chichester, U.K.

Bronold, M., Tomm, Y., and Jaegermann, W. (1994) Surface states on cubic d-band semiconductor pyrite (FeS_2). Surface Science, 314, L931–L936.

Bullett, D.W. (1982) Electronic structure of 3d pyrite- and marcasite-type sulphides. Journal of Physics C: Solid State Physics, 15, 6163–6174.

Burns, R.G. and Vaughan, D.J. (1970) Interpretation of the reflectivity behaviour of ore minerals. In C. Karr Jr., Ed., Infrared and Raman Spectroscopy of Lunar and Terrestrial Minerals, 514p. New York, Academic, New York.

Eyert, V., Höck, K.-H., Fiechter, S., and Tributsch, H. (1998) Electronic structure of FeS_2: the crucial role of electron-lattice interaction. Physical Review B, 57, 6350–6359.

Folkerts, W., Sawatzky, G.A., Haas, C., de Groot, R.A., and Hillebrecht, F.U. (1987) Electronic structure of some 3D transiton-metal pyrites. Journal of Physics C: Solid State Physics, 20, 4135–4144.

Gelius, V. (1974) Recent progress in ESCA studies of gases. Journal of Electron Spectroscopy and Related Phenomena, 5, 985–1057.

Goodenough, J.B. (1972) Energy bands in TX_2 compounds with pyrite, marcasite and arsenopyrite structures. Journal of Solid State Chemistry, 5, 144–152.

Holzwarth, N.A., Harris, S., and Liang, K.S. (1985) Electronic structure of RuS_2. Physical Review B, 32, 3745–3752.

Hüfner, S. (1995) Photoelectron Spectroscopy, 516 p. Springer, Berlin.

Kühne, H.-M., Jaegermann, W., and Tributsch, H. (1984) The electronic band character of Ru dichalcogenides and its significance for the photoelectrolysis of water. Chemical Physics Letters, 112, 160–164.

Kurmaev, E., van Ek,J., Ederer, D.L., Zhou, L., Callcott, T.A., Perera, R.C.C., Cherkashenko, V.M., Shamin, S.N., Trofimova, V.A., Bartkowski, S., Neumann, M., Fujimori, A., and Moloshag, V.P. (1998) Experimental and theoretical investigation of the electronic structure of transition metal sulphides: CuS, FeS_2 and $FeCuS_2$. Journal of Physics: Condensed Matter, 10, 1687–1697.

Lad, R.J. and Henrich, V.E. (1989) Photoemission study of the valence-band electronic structure of Fe_xO, Fe_3O_4, and α-Fe_2O_3 single crystals. Physical Review B, 39, 13478–13485.

Lauer, S., Trautwein, A.X., and Harris, F.E. (1984) Electronic-structure calculations, photoelectron spectra, optical spectra, and Mössbauer parameters for the pyrites MS_2 (M = Fe, Co, Ni, Cu, Zn). Physical Review B, 29, 6774–6783.

Li, E.K., Johnson, K.H., Eastman, D.E., and Feehouf, J.L. (1974) Localized and bandlike valence-electron states in FeS_2 and NiS_2. Physical Review Letters, 9, 470–472.

Leiro, J.A., Laajalehto, K., Kartio, I., and Heinonen, M.H. (1998) Surface core-level shift and phonon broadening in PbS (100). Surface Science, 412/413, L918–L923.

Mycroft, J.R., Bancroft, G.M., McIntyre, N.S., Lorimer, J.W., and Hill, I.R. (1990) Detection of sulphur and polysulphides on electrochemically oxidized pyrite surfaces by X-ray photoelectron spectroscopy and Raman spectroscopy. Journal of Electroanalytical Chemistry, 292, 139–152.

Mycroft, J.M., Nesbitt, H.W., and Pratt, A.R. (1995) X-ray photoelectron and Auger electron spectroscopy of air-oxidized pyrrhotite: distribution of oxidized species with depth. Geochimica Cosmochimica Acta, 59, 721–733.

Nesbitt, H.W., Bancroft, G.M., Pratt, A.R., and Scaini, M.J. (1998) Sulfur and iron surface states on fractured pyrite surfaces. American Mineralogist, 83, 1067–1076.

Nesbitt, H.W., Scaini, M., Hoechst, H., Brancroft, G.M., Schaufuss, A.G., and Szargan, R. (2000) Synchrotron XPS evidence for Fe^{2+}-S and Fe^{3+}-S surface species on pyrite fracture surfaces and their 3d electronic states. American Mineralogist, 85, 850–857.

Nesbitt, H.W., Uhlig, I., and Szargan, R. (2002) Surface reconstruction and As-polymerization at fractured loellingite surfaces. American Mineralogist, 87, 1000–1004.

Nesbitt, H.W., Uhlig, I., Bancroft, G.M., and Szargan, R. (2003) Resonant XPS study of the pyrite valence band with implications for molecular orbital contributions. American Mineralogist, 88, 1279–1286.

Pettenkofer, C., Jaegermann, W., and Bronold, M. (1991) Site specific surface interaction of electron donors and acceptors on FeS_2 (100) cleavage planes. Berichte der Bunsen-Gesellschaft für Physikalische Chemie, 95, 560–565.

Raybaud, P., Hafner, J, Kresse, G., and Taulhoat, H. (1997) *Ab initio* density functional studies of transition-metal sulphides: II. Electronic structure. Journal of Physics: Condensed Matter, 9, 11107–11140.

Rosso, K.M., Becker, U., and Hochella, M.F. (1999) The interaction of pyrite {100} surfaces with O_2 and H_2O: Fundamental oxidation mechanisms. American Mineralogist, 84, 1549–1561.

Schaufuss, A.G., Nesbitt, H.W., Scaini, M.J., Höchst, H., Bancroft, G.M., and Szargan, R. (2000) Reactivity of surface sites on fractured arsenopyrite (FeAsS) toward oxygen. American Mineralogist, 85, 1754–1766.

Sherman, D.M. (1985) The electronic structures of Fe^{3+} coordination sites in iron oxides: Applications to spectra, bonding and magnetism. Physics and Chemistry of Minerals, 12, 161–175.

Shirley, D.A., (1972) High-resolution X-ray photoemission spectrum of the valence bands of gold. Physical Review B, 5, 4709–4714.

Tanuma, S., Powell, C.J., and Penn, D.R. (1991) Calculations of electron inelastic mean free paths III. Surface and Interfacial Analysis, 17, 927–939.

Temmerman, W.M., Durham, P.J., and Vaughan, D.J. (1993) The electronic structures of the pyrite-type disulphides (MS_2, where M = Mn, Fe, Co, Ni, Cu, Zn) and the bulk properties of pyrite from Local Density Approximation (LDA) band structure calculations. Physics and Chemistry of Minerals, 20, 248–254.

Todd, E.C., Sherman, D.M., and Purton, J.A. (2003) Surface oxidation of pyrite under ambient atmospheric and aqueous (pH = 2 to 10) conditions: Electronic structure and mineralogy from X-ray absorption spectroscopy. Geochimica et Cosmochimica Acta, 67, 881–893.

van der Heide, H., Hemmel, R., van Bruggen, C.F., and Haas, C. (1980) X-ray photoelectron spectra of 3d transition metal pyrites. Journal of Solid State Chemistry, 33, 17–25.

Yeh, J.J. and Lindau, I. (1985) Atomic Data and Nuclear Data Tables (32). Academic Press, Oxford.

MANUSCRIPT RECEIVED JANUARY 27, 2003
MANUSCRIPT ACCEPTED JULY 7, 2003
MANUSCRIPT HANDLED BY JAMES KUBICKI